



Modulation of hydroxyl variability by ENSO in the absence of external forcing

Alexander J. Turner^{a,b,1}, Inez Fung^a, Vaishali Naik^c, Larry W. Horowitz^c, and Ronald C. Cohen^{a,b}

^aDepartment of Earth and Planetary Sciences, University of California, Berkeley, CA 94720; ^bCollege of Chemistry, University of California, Berkeley, CA 94720; and ^cGeophysical Fluid Dynamics Laboratory, National Oceanic and Atmospheric Administration (NOAA), Princeton, NJ 08540

Edited by Mark H. Thiemens, University of California at San Diego, La Jolla, CA, and approved July 27, 2018 (received for review May 1, 2018)

The hydroxyl radical (OH) is the primary oxidant in the troposphere, and the impact of its fluctuations on the methane budget has been disputed in recent years, however measurements of OH are insufficient to characterize global interannual fluctuations relevant for methane. Here, we use a 6,000-y control simulation of preindustrial conditions with a chemistry-climate model to quantify the natural variability in OH and internal feedbacks governing that variability. We find that, even in the absence of external forcing, maximum OH changes are $3.8 \pm 0.8\%$ over a decade, which is large in the context of the recent methane growth from 2007–2017. We show that the OH variability is not a white-noise process. A wavelet analysis indicates that OH variability exhibits significant feedbacks with the same periodicity as the El Niño–Southern Oscillation (ENSO). We find intrinsically generated modulation of the OH variability, suggesting that OH may show periods of rapid or no change in future decades that are solely due to the internal climate dynamics (as opposed to external forcings). An empirical orthogonal function analysis further indicates that ENSO is the dominant mode of OH variability, with the modulation of OH occurring primarily through lightning NO_x . La Niña is associated with an increase in convection in the Tropical Pacific, which increases the simulated occurrence of lightning and allows for more OH production. Understanding this link between OH and ENSO may improve the predictability of the oxidative capacity of the troposphere and assist in elucidating the causes of current and historical trends in methane.

hydroxyl | ENSO | La Niña | methane | tropospheric oxidative capacity

The hydroxyl radical (OH) is the primary oxidant for many non- CO_2 greenhouse gases (GHGs), such as methane, as well as a number of ozone-depleting substances (1, 2). As such, the burden and distribution of OH dictates the lifetime of many important atmospheric trace gases and will affect the global warming potential of many GHGs. However, we currently lack a predictive understanding of OH variability on decadal-to-centennial timescales, evidenced by the disagreement between global models in their simulation of OH trends (e.g., ref. 3). For example, Naik et al. (3) found large intermodel diversity in both the sign and magnitude of preindustrial to present-day OH changes, ranging from -12% to $+14\%$.

Efforts to characterize the factors that control global mean OH have generally focused on the ozone photolysis frequency (J_{O_3}), specific humidity (q), sources of reactive nitrogen (S_N ; i.e., NO_x), and sources of reactive carbon (S_C ; e.g., methane, CO, and NMVOCs) (e.g., refs. 5–7). Specifically, Murray et al. (7) compared simulations of preindustrial and present-day conditions to derive the following relationship:

$$[\text{OH}] \propto J_{\text{O}_3} q \frac{S_N}{S_C^{3/2}}. \quad [1]$$

The dependence on J_{O_3} and q is because production of OH on global scales is due to the photolysis of ozone in the presence of water vapor, dependence on S_N is because increases in NO_x

result in faster recycling of OH via reaction of HO_2 or RO_2 with NO, and OH is inversely related with S_C because the dominant loss process for OH involves reactions with CO, methane, and NMVOCs. This relationship from Murray et al. (7) highlights the major factors that could drive changes in global mean OH.

Previous work from Turner et al. (8) and Rigby et al. (9) has shown how relatively small variations in OH (on the order of $\sim 3\%$ over a 10-y period) can explain present trends in atmospheric methane; however, direct measurements of OH are neither sufficiently precise nor spatially dense enough to characterize global OH variations of this magnitude. Instead, previous work has used measurements of methyl chloroform (CH_3CCl_3) to indirectly estimate the global OH burden, since OH is the primary oxidant for methyl chloroform and the oxidation is slow enough to represent a global integral (e.g., refs. 10–13). Many of these previous studies have found OH to be well buffered (e.g., refs. 13–15). This has led to a number of recent studies assuming that OH is time-invariant (i.e., no interannual variability) when analyzing methane trends (e.g., refs. 16 and 17).

Previous work has identified the importance of the El Niño–Southern Oscillation (ENSO) in tropospheric ozone (e.g., refs. 18–20); however, there has been little work discussing the relationship between ENSO and OH. A notable exception is the work of Prinn et al. (10, 11), who discuss how ENSO may have impacted their methyl chloroform measurements at Samoa due to its location in the Western Pacific. They suggest a tentative link between warm, cloudy El Niño events and low OH. Krol and Lelieveld (21) also mention the impact of biomass burning on OH during El Niño. Here we use a coupled chemistry-climate

Significance

The hydroxyl radical (OH) is central to tropospheric chemistry, but current measurements are insufficient to assess its effects on year-to-year changes in atmospheric methane. We use a 6,000-y control simulation in a global coupled chemistry-climate model to study the natural variability of OH. We find that natural OH variability can produce (unforced) methane trends as large as the observed changes in methane over the last few decades. Additionally, we find a link between OH and La Niña. While we cannot directly measure annual global mean OH, we can use what we know about La Niña to improve our understanding of OH. This may, in turn, improve our understanding of recent methane trends.

Author contributions: A.J.T. designed research; A.J.T. performed research; V.N. and L.W.H. developed and ran the model; A.J.T., I.F., and R.C.C. analyzed data; A.J.T. wrote the paper; and I.F., V.N., L.W.H., and R.C.C. provided comments on the paper.

The authors declare no conflict of interest.

This article is a PNAS Direct Submission.

This open access article is distributed under Creative Commons Attribution-NonCommercial-NoDerivatives License 4.0 (CC BY-NC-ND).

¹To whom correspondence should be addressed. Email: alexjturner@berkeley.edu.

This article contains supporting information online at www.pnas.org/lookup/suppl/doi:10.1073/pnas.1807532115/-DCSupplemental.

Published online August 20, 2018.

model to demonstrate how ENSO can induce OH variability and trends that are large enough to explain present trends in atmospheric methane even in the absence of changes in methane emissions.

Methods and Results

We use a 6,000-y preindustrial control simulation conducted with the Geophysical Fluid Dynamics Laboratory CM3 (GFDL-CM3) model. GFDL-CM3 incorporates an atmospheric chemistry model within the framework of the atmosphere, ocean, land, and sea-ice components (3, 22–24). Most pertinent to our application is the fully coupled tropospheric and stratospheric

chemistry. The merged chemical scheme includes tropospheric chemistry based on MOZART-2 (Model for Ozone and Related chemical Tracers; ref. 25; simulates atmospheric concentrations of 97 chemical species including aerosols) and stratospheric chemistry based on AMTRAC (Atmospheric Model with Transport and Chemistry; ref. 26). The isoprene mechanism in GFDL-CM3 does not include OH recycling pathways discussed in Taraborrelli et al. (27), and modifying the chemistry scheme to include the OH recycling mechanisms from isoprene oxidation could alter the OH variability in the model. GFDL-CM3 uses a cubed sphere grid with 48×48 cells per face, resulting in a native horizontal resolution ranging from ~ 163 km to

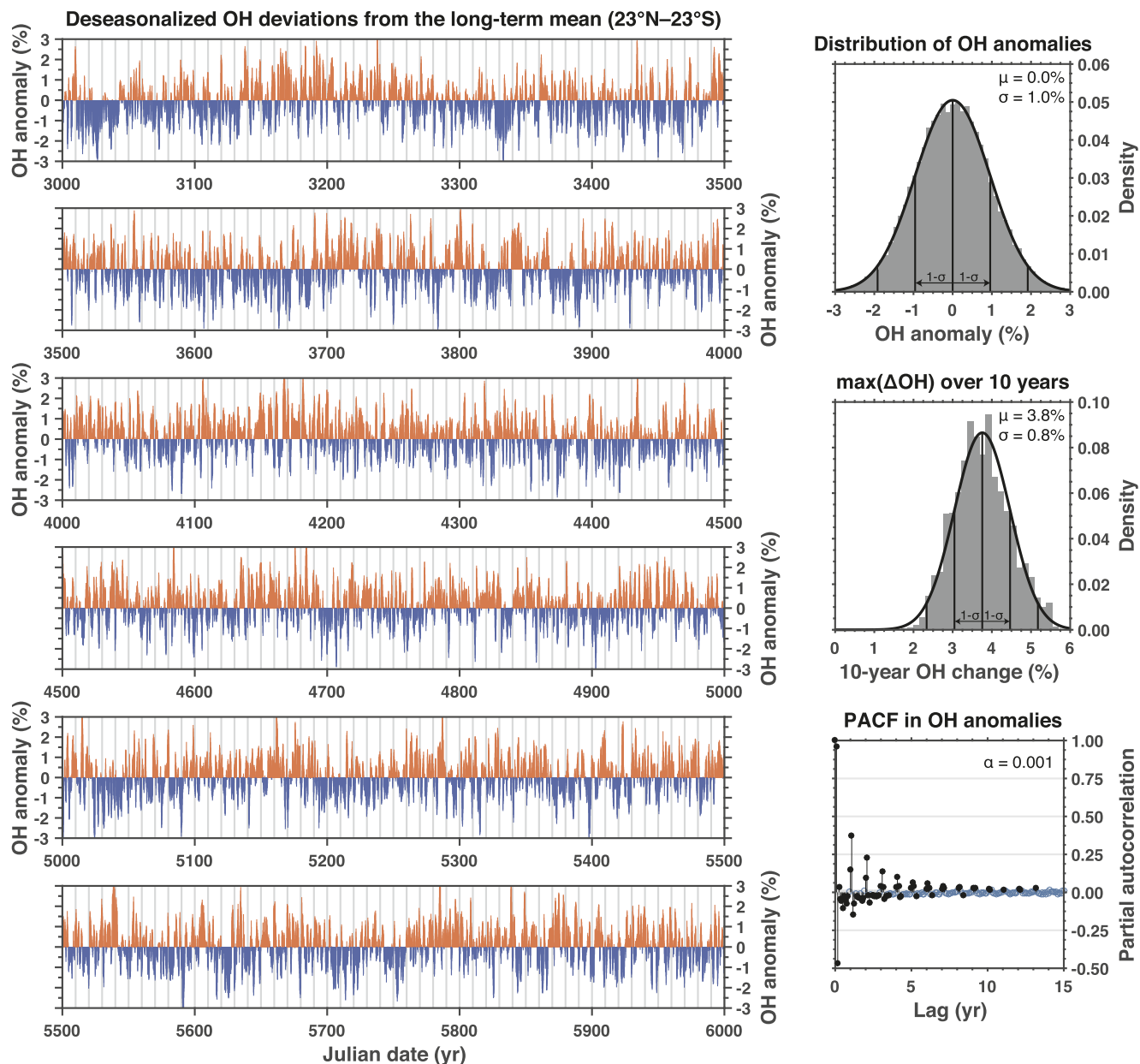


Fig. 1. Statistics of OH anomalies in a preindustrial control simulation. *Left* shows the monthly OH anomalies in the tropics (23°N – 23°S) from years 3,000 to 6,000 in the GFDL-CM3 control run. OH anomalies are the deseasonalized OH deviations (pressure-weighted mean, 300 to 800 hPa) from the long-term mean, normalized to the long-term mean, and expressed as a percentage: $(x - \bar{x}) \cdot \bar{x}^{-1}$. Seasonal cycle is removed using a stable seasonal filter. *Top Right* shows the distribution of OH anomalies (gray bars) and a normal distribution fitted to the anomalies (black line). *Middle Right* is the maximum change in OH over a 10-y period (gray bars) and a normal distribution fitted to ΔOH (black line). *Bottom Right* is the partial autocorrelation function (PACF) of the OH anomalies; filled black circles indicate significant lags ($\alpha = 0.001$).

~231 km with 48 vertical layers. Results analyzed here are at monthly time resolution regridded to a horizontal resolution of $2^\circ \times 2.5^\circ$. This control simulation holds all forcings constant and uses prescribed (static) vegetation. Specifically, the land use and land cover, tropospheric ozone precursor emissions, solar and volcanic forcings, and GHG concentrations (including methane) are held at 1860 conditions. Production of NO_x by lightning is parameterized as a function of convective cloud-top height and thus varies with the model meteorology. Changes in stratospheric ozone concentrations can impact the photolysis in the troposphere. GFDL-CM3 has been shown to have a reasonable simulation of ENSO based on CMIP5 intercomparisons (28–34). The ENSO period is slightly short (~ 2.5 y), and its anomaly patterns and teleconnections tend to be shifted slightly west of observed [see figure 18 in Donner et al. (22)].

Fig. 1 shows the time series of the deseasonalized OH anomalies in the tropics (23°N – 23°S) from years 3,000 to 6,000 in the control simulation. We use pressure-weighted tropospheric mean quantities from 300 to 800 hPa. [Boundary layer is excluded because concentrations of methane are prescribed below 800 hPa, which may dampen the potential variability and feedbacks. Using the full tropospheric column makes little difference in the periodicity (see *SI Appendix*, Fig. S1).] The first 3,000 y of the control simulation are discarded due to a climate drift of $\sim 1^\circ\text{C}$ temperature increase and a change in computer architecture in year 1,070 of the control simulation that resulted in a $\sim 4\%$ increase in global mean OH (see *SI Appendix*, Fig. S2). From Fig. 1, we find an OH interannual variability of $\pm 1.0\%$

($1-\sigma$). This variability is consistent with previous work that finds global mean OH to be well buffered [e.g., Montzka et al. (13), who infer an interannual variability of $2.3 \pm 1.5\%$ using observations of methyl chloroform]. However, the present atmosphere is substantially NO_x -richer than the preindustrial, and we may expect more OH recycling in the present. A qualitative examination of the OH anomaly time series shows regular excursions to $\pm 2\%$ for individual decades. These excursions could lead to transients in the atmospheric record for molecules whose atmospheric lifetime is dictated by OH, such as methane. To determine the distribution of decadal-scale changes in OH, we randomly draw decades from this 3,000-y control simulation and compute the maximum change in OH over a decade (ΔOH). We find ΔOH over a decade is $3.8 \pm 0.8\%$ (see Fig. 1, *Middle Right*). These changes in OH alone are large enough to explain present trends in methane, independent of changes in methane sources.

The distribution of decadal changes in OH provides evidence of atmospherically relevant changes in OH in the absence of external forcing. However, it does not indicate whether this simply arises from random sampling of a white-noise process or if there is a mechanism that could provide longer term feedbacks. To investigate the possibility of feedbacks, we compute the partial autocorrelation function (PACF) of the OH anomalies. Black dots in Fig. 1, *Bottom Right* indicate lags that are significant at the 99.9% level ($\alpha = 0.001$). We find numerous significant, large lags between 0 and 5 y as well as significant, but weaker, lags going out 10+ y. This indicates that there are feedbacks in

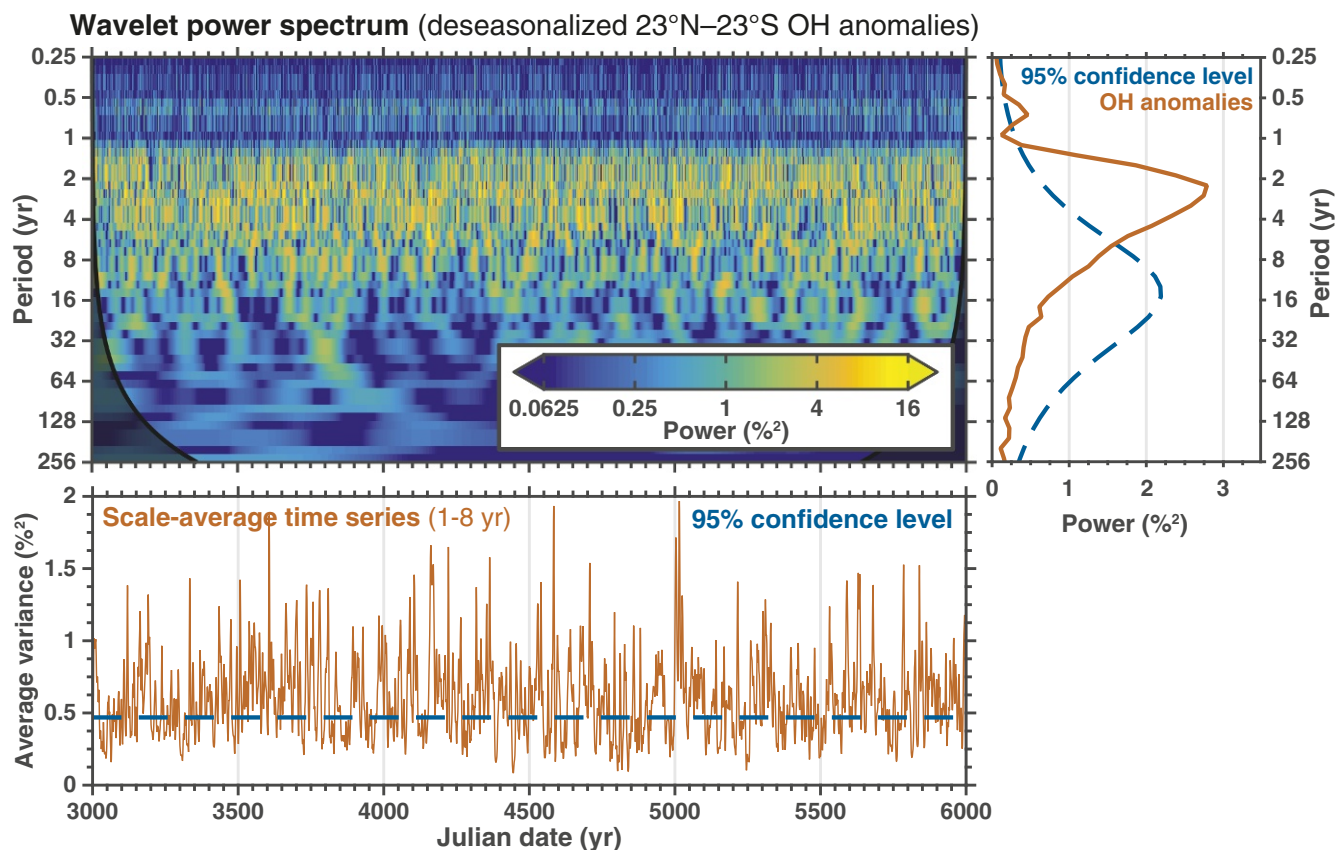


Fig. 2. Wavelet analysis of the OH anomalies (300 to 800 hPa) in a preindustrial control simulation. *Top Left* is the bias-rectified local wavelet power spectrum of the OH anomalies from Fig. 1 using a Morlet wavelet following Torrence and Compo (4). Left axis is the Fourier period (in years), bottom axis is time (in years), and shading is the power (in $\%^2$). *Right* is the global wavelet spectrum for the OH anomalies (solid red line) and the 95% confidence level (dashed blue line) assuming red noise. *Bottom* is the scale-averaged wavelet power over the 1–8 y band for the OH anomalies (solid red line) and the 95% confidence level (dashed blue line) assuming red noise.

